pounds $[Fe(TPP)(TMSO_2)]^+$ (1.2 mm s^{-1})[35] and $[Fe(TPP)(H_2O)_2]^+$ (1.6 mm s^{-1})[20] and slightly smaller than that in the six-coordinate, spin-mixed, monoclinic form of $[Fe(OEP)(3\text{-}Cl\text{-}py)_2]^+$ (2.7 mm s^{-1}).[5] The contact-field parameter in compound **1**, B_0^c = 17 T, is about 1.5 T below the low-field side of the range of internal fields in high-spin heme derivatives[35] but is considerably larger than the value of 12 T deduced from low-temperature Mössbauer spectra in spin-mixed Chromatium ferricytochrome c′ (pH 7.8)[25] and in $[Fe(OEP)(3\text{-}Cl\text{-}py)]^+$ dimers.[36] The values of the g factors and zero-field-splitting and A-tensor components in compound **1** resemble those in the protein states I and II of *Rhodospirillum rubrum* ferricytochrome c′.[37] The quadrupole splitting in compound **1**, however, is significantly larger than the values ΔE_Q = 1.35 and 1.65 mm s^{-1} in the two protein states I and II, respectively.

Summing up the magnetic, electronic, and structural data, we conclude that the (triflato) aquoiron(III) "picket-fence" porphyrin compound **1** has a weakly spin-mixed ground state, with slightly more $S = {}^3/_2$ character than in high-spin ferric porphyrin derivatives.

Acknowledgment. R.W. is the recipient of an Alexander von Humboldt Award and thanks the Alexander von Humboldt Foundation for financial support. We thank Dr. Jacobi and Professor Gütlich from the Institut für Anorganische und Analytische Chemie, Johannes Gutenberg Universität, Mainz, FRG, for performing the magnetic susceptibility measurements.

Supplementary Material Available: Tables SI-SIV, listing thermal parameters for anisotropic atoms, hydrogen atom positions and thermal parameters, complete bond distances, and complete bond angles (11 pages); Table SV, listing observed and computed structure factor amplitudes (×10) for all observed reflections (19 pages). Ordering information is given on any current masthead page.

(35) Mashiko, T.; Kastner, M. E.; Spartalian, K.; Scheidt, W. R.; Reed, C. A. *J. Am. Chem. Soc.* **1978**, *100*, 6354.
(36) Gupta, G. P.; Lang, G.; Scheidt, W. R.; Geiger, D. K.; Reed, C. A. *J. Chem. Phys.* **1986**, *85*, 5212.
(37) Emptage, M. H.; Zimmermann, R.; Que, L.; Münck, E.; Hamilton, W. D.; Orme-Johnson, W. H. *Biochim. Biophys. Acta* **1977**, *495*, 12.

Contribution from the Department of Chemistry, University of Houston, Houston, Texas 77204-5641

Electrochemistry, Spectroscopy, and Reactivity of (*meso*-Tetrakis(1-methylpyridinium-4-yl)porphinato)cobalt(III,II,I) in Nonaqueous Media

C. Araullo-McAdams and K. M. Kadish*

Received January 23, 1989

The spectral and electrochemical properties of (*meso*-tetrakis(1-methylpyridinium-4-yl)porphinato)cobalt(II), $[(TMpyP)Co]^{4+}$, were investigated in dimethylformamide, dimethyl sulfoxide, and pyridine. A single one-electron oxidation of the complex involves a conversion of Co(II) to Co(III) and occurs in the range of +0.29 to −0.01 V vs SCE. Up to four electroreduction processes are also observed, and $[(TMpyP)Co]^{4+}$ can be reduced by a total of six electrons to generate $[(TMpyP)Co]^{2-}$ as a final product. The first reduction occurs between −0.49 and −0.61 V and leads to $[(TMpyP)Co^{I}]^{3+}$. The second reduction involves an addition of one electron to the porphyrin π-ring system and produces $[(TMpyP)Co^{I}]^{2+}$. However, electrochemical, spectroelectrochemical, and ESR monitoring of this reaction give data consistent with the occurrence of an intramolecular electron transfer involving electrogenerated $[(TMpyP)Co^{I}]^{2+}$ to form $[(TMpyP)Co^{II}]^{2+}$ in solution. Two additional reactions of $[(TMpyP)Co]^{2+}$ occur at $E_{1/2}$ values between −0.89 and −1.10 V, and these involve an overall four-electron reduction of the four *N*-methylpyridiniumyl substituents on TMpyP. The axial ligand binding reactions of pyridine with $[(TMpyP)Co]^{5+}$, $[(TMpyP)Co]^{4+}$, $[(TMpyP)Co]^{3+}$, and $[(TMpyP)Co]^{2+}$ were monitored by electrochemistry and ESR spectroscopy, and the ESR spectra of $[(TMpyP)Co(S)]^{4+}$, $[(TMpyP)Co(py)(S)]^{4+}$, $[(TMpyP)Co(py)_2]^{4+}$, $[(TMpyP)Co(py)]^{2+}$ and $[(TMpyP)Co(py)_2]^{2+}$ are presented where S = DMF or Me_2SO.

Introduction

The electroreduction of numerous cobalt porphyrins in nonaqueous media has been described in the literature.[1-12] The most prevalent reduction mechanism, which occurs in virtually all cases, involves a direct electron addition at the Co(II) center to form a Co(I) complex. A second electron is then added to the porphyrin π-ring system and leads to formation of a cobalt(I) porphyrin π anion radical.

The only cobalt(I) porphyrin dianion that has been characterized is $[((CN)_4TPP)Co]^{3-}$. This compound is electrogenerated from $((CN)_4TPP)Co$ and proceeds via an initial one-electron addition to the porphyrin π-ring system to form a cobalt(II) anion radical.[8] The potential for this reaction varies between −0.24 and −0.51 V depending upon solvent and is anodically shifted by as much as 1600 mV with respect to the first π-ring-centered reduction of (TPP)Co under the same solution conditions. The second reduction of $((CN)_4TPP)Co$ involves the Co(II) center and generates the cobalt(I) porphyrin π anion radical at $E_{1/2}$ values between −0.80 and −0.94 V. The third one-electron reduction occurs at −1.72 to −1.78 V and generates the Co(I) dianion. This reaction is very well-defined and has been characterized in a number of solvents.[8]

Several other easily reducible metalloporphyrins have been investigated in non-aqueous media. $[(TMpyP)M]^{4+}$ complexes, where TMpyP is *meso*-tetrakis(1-methylpyridinium-4-yl)porphyrin and M = Zn(II), Cu(II), or VO, are monomeric in DMF and can be reversibly reduced by a total of six electrons in three steps.[13] The first reduction involves a two-electron transfer at the porphyrin π-ring system and occurs at potentials that are positively shifted

(1) Kadish, K. M. *Prog. Inorg. Chem.* **1986**, *34*, 435-605.
(2) Guilard, R.; Kadish, K. M. *Chem. Rev.* **1988**, *88*, 1121-1146.
(3) Giraudeau, A.; Callot, H. J.; Jordan, J.; Ehzar, I.; Gross, M. *J. Am. Chem. Soc.* **1979**, *101*, 3857.
(4) Dolphin, D.; Halko, D. J.; Johnson, E. *Inorg. Chem.* **1981**, *20*, 2982.
(5) Wolberg, A.; Manassen, J. *J. Am. Chem. Soc.* **1970**, *92*, 2982.
(6) Walker, F. A.; Beroiz, D.; Kadish, K. M. *J. Am. Chem. Soc.* **1976**, *98*, 3484.
(7) Felton, R. H.; Linschitz, J. *J. Am. Chem. Soc.* **1966**, *88*, 1113.
(8) Lin, X. Q.; B.-Cocolios, B.; Kadish, K. M. *Inorg. Chem.* **1986**, *25*, 3242.
(9) Kadish, K. M.; Mu, X. H.; Lin, X. Q. *Inorg. Chem.* **1988**, *27*, 1489.
(10) Truxillo, L. A.; Davis, D. G. *Anal. Chem.* **1975**, *47*, 2260.
(11) Kadish, K. M.; Bottomley, L. A.; Beroiz, D. *Inorg. Chem.* **1978**, *17*, 1124.
(12) Kadish, K. M.; Bottomley, L. A.; Kelly, S.; Schaeper, D.; Shiue, L. R. *Bioelectrochem. Bioenerg.* **1981**, *8*, 213.
(13) Kadish, K. M.; Araullo, C.; Maiya, C. G.; Sazou, D.; Barbe, J.-M.; Guilard, R., *Inorg. Chem.* **1989**, *28*, 2528.

0020-1669/90/1329-2749$02.50/0

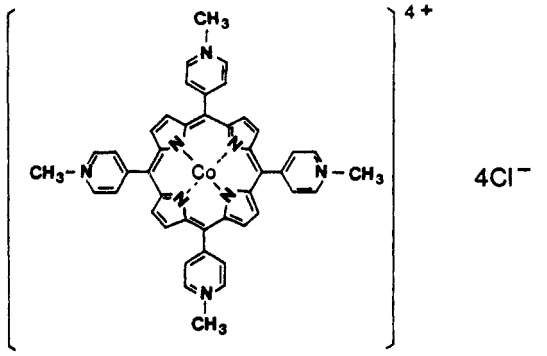

Figure 1. Structure of (TMpyP)$CoCl_4$.

by up to 1150 mV with respect to $E_{1/2}$ for reduction of (TPP)M species having the same central metal. The electrode reactions of $[(TMpyP)Mn]^{5+}$ and $[(TMpyP)Ni]^{4+}$ have also been investigated in DMF. The Ni(II) complex exists in a monomer–dimer equilibrium[14] and is reduced in four steps while the Mn(III) porphyrin[15] is monomeric and undergoes three reduction steps.

This present work examines the spectroscopy, electrochemistry, and ligand-binding reactions of neutral, oxidized, and reduced (*meso*-tetrakis(1-methylpyridinium-4-yl)porphinato)cobalt(II), $[(TMpyP)Co]^{4+}$, whose structure is shown in Figure 1. The thin-layer spectroelectrochemistry associated with a reduction of $[(TMpyP)Co]^{5+}$ to give $[(TMpyP)Co]^{4+}$ in water was first reported in 1977,[16] and more recently, $[(TMpyP)Co]^{5+}$ was used as a catalyst in the reduction of oxygen to hydrogen peroxide.[17,18] All three studies were carried out in aqueous media, and only the Co(III)/Co(II) redox couple was investigated under these experimental conditions.

Electrochemical data on $[(TMpyP)Co]^{4+}$ are unavailable in non-aqueous media, and it was thus not clear whether $[(TMpyP)Co]^{4+}$ would undergo a reduction mechanism similar to that of $[(TMpyP)M]^{4+}$ complexes with electroinactive central metals[13,14] or to that of other cobalt metalloporphyrins such as those in the octaethylporphyrin (OEP) or tetraphenylporphyrin (TPP) series. This question is answered in the present paper, which investigates the first electron-transfer and ligand-binding reactivity of neutral, oxidized, and reduced $[(TMpyP)Co]^{4+}$ in non-aqueous media. Each of the reactions were investigated in dimethylformamide (DMF), dimethyl sulfoxide (Me_2SO), and pyridine (py). ESR and thin-layer spectroelectrochemical methodologies were used to provide spectral characterization of the neutral, electrooxidized, and electroreduced species, and an overall electron-transfer sequence is presented.

Experimental Section

Chemicals. Tetra-*n*-butylammonium perchlorate (TBAP), purchased from Sigma Chemical Co., was recrystallized from ethyl alcohol and dried in a vacuum oven at 40 °C for at least 1 week prior to use. DMF and Me_2SO were vacuum distilled over 4-Å molecular sieves while spectroscopic grade py was distilled over calcium hydride.

Free base $[(TMpyP)H_2]^{4+}$ and (TMpyP)$CoCl_4$ were synthesized according to procedures reported in the literature.[19,20]

Instrumentation and Methods. UV–visible spectra of the initial complexes were recorded with an IBM 9430 spectrophotometer. ESR spectra were recorded with an IBM Model ER-100D electron spin resonance system. ESR measurements of the reduced complexes were taken after controlled-potential electrolysis under an inert atmosphere. The reduced samples were transferred to an ESR cell, which was modified for use on a Schlenk line, and then immediately frozen in liquid nitrogen.

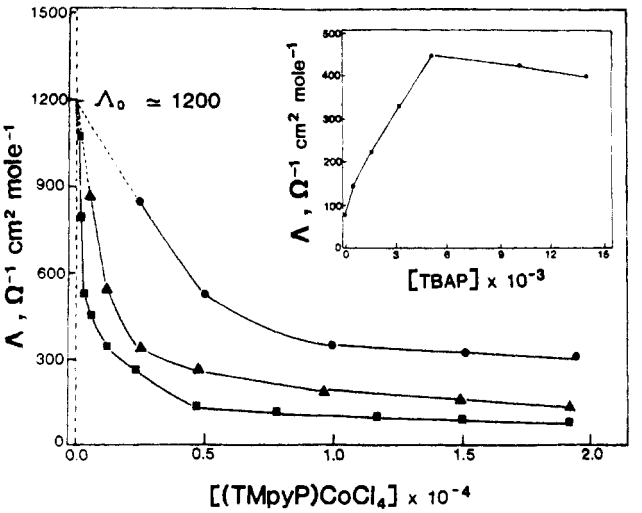

Figure 2. Molar conductance of (TMpyP)$CoCl_4$ in DMF without TBAP (■) and in DMF containing 0.001 (▲) or 0.01 M TBAP (●). The inset of the figure shows the variation of molar conductance for 1×10^{-4} M (TMpyP)$CoCl_4$ as a function of [TBAP].

Platinum was used for both the working and counter electrodes in cyclic voltammetric and polarographic experiments. A platinum minigrid electrode was used in the thin-layer spectroelectrochemical cell, the design of which is described in the literature.[21] Cyclic voltammetry, polarography, and thin-layer controlled-potential coulometry were carried out on an IBM EC 225 voltammetric analyzer coupled with an Omnigraphic Houston 9002A X-Y recorder. A Princeton Applied Research EG & G Model 174A/175 polarographic analyzer/potentiostat was used for bulk controlled-potential coulometry experiments. Potentials were measured and reported against a saturated calomel electrode (SCE), which was separated from the bulk solution by means of a fritted-glass disk junction.

Thin-layer spectroelectrochemical measurements were made with an IBM EC 225 voltammetric analyzer coupled with a Tracor Northern 6500 spectrometer/multichannel analyzer. A Xenon arc lamp was used as the light source. A long pass filter was used as a UV cutoff since a photochemical decomposition of this porphyrin was observed to occur upon prolonged irradiation by UV light.

Conductances of the degassed porphyrin solutions were obtained by using a homemade conductivity cell in conjunction with a Yellowstone International Model 31 conductivity bridge. The measured cell constant is 0.216 cm^{-1}, and the cell was calibrated with various concentrations of high-purity KCl solutions.

Results and Discussion

Characterization of Neutral (TMpyP)$CoCl_4$. (TMpyP)$CoCl_4$ is totally dissociated in aqueous media[20] and gives the tetracationic Co(II) species as shown in eq 1. The dissociation of

$$(TMpyP)CoCl_4 \rightleftarrows [(TMpyP)Co]^{4+} + 4Cl^- \qquad (1)$$

(TMpyP)$CoCl_4$ is not complete in DMF, Me_2SO, or py but rather varies with both the porphyrin concentration and the presence of TBAP supporting electrolyte. This is illustrated by the data in Figure 2, which shows the molar conductance of (TMpyP)$CoCl_4$ as a function of porphyrin concentration in DMF containing various amounts of TBAP between 10^{-4} and 10^{-2} M.

Only about 6% of a 1×10^{-4} M (TMpyP)$CoCl_4$ solution is dissociated in neat DMF[22] and the molar conductance (Λ) under these solution conditions is 80 Ω^{-1} cm^2 mol^{-1}. However, the molar conductance of 1.0×10^{-4} M (TMpyP)$CoCl_4$ increases as a

(14) Kadish, K. M.; Sazou, D.; Liu, Y. M.; Saoiabi, A.; Ferhat, M.; Guilard, R. *Inorg. Chem.* **1988**, *27*, 686.
(15) Hambright, P.; Williams, R. F. In *Porphyrin Chemistry Advances*; Longo, F. R., Ed.; Ann Arbor Sciences: Ann Arbor, MI, 1979; pp 284–292.
(16) Rohrbach, D. F.; Deutsch, E.; Heineman, W. R.; Pasternack, R. F. *Inorg. Chem.* **1977**, *16*, 2650.
(17) Chan, R. J.-H.; Uedo, C. C.; Kuwana, T. *J. Am. Chem. Soc.* **1983**, *105*, 3713.
(18) Chan, R. J.-H.; Su, O.; Kuwana, T. *Inorg. Chem.* **1985**, *24*, 3777.
(19) Pasternack, R. F.; Huber, P. R.; Boyd, P.; Engasser, G.; Francesconi, L.; Giggs, E.; Fasella, P.; Ventura, G. C.; Hinds, L de C. *J. Am. Chem. Soc.* **1972**, *94*, 4511.
(20) Evans, D. F.; Wood, D. *J. Chem. Soc., Dalton Trans.* **1987**, 3909.
(21) Lin, X. Q.; Kadish, K. M. *Anal. Chem.* **1985**, *57*, 1498.
(22) The degree of dissociation is given by Λ/Λ_0 where Λ is the molar conductance at a certain substrate concentration and Λ_0 is the molar conductance at infinite dilution.[23] The value for Λ_0 is obtained from the plot shown in Figure 2 and the extrapolated value of Λ_0 is about 1200 Ω^{-1} cm^2 mol^{-1}.
(23) Shedlovsky, T. and Shedlovsky, L. In *Techniques of Chemistry, Physical Methods of Chemistry*; Weissberger, A., Rossiter, B. W., Eds.; Wiley-Interscience: New York, 1971; Vol. I, Part IIA, Chapter 3.

Table I. ESR Parameters of $[(TMpyP)Co]^{4+}$ and Its Electroreduced Products at −150 °C

solvent[a]	[py], M	electrolysis conditions	ESR-active species	g values[b]	A values,[b] G
DMF	0	none[c]	$[(TMpyP)Co(DMF)]^{4+}$	$g_\perp = 2.335$; $g_\parallel = 2.061$	$A_\parallel = 83$
		−1.2 V	$[(TMpyP)Co(DMF)]^{2-}$	$g_\perp = 2.341$; $g_\parallel = 1.992$	$A_\parallel = 88$
	2.0	none[c]	$[(TMpyP)Co(DMF)(py)]^{4+}$	$g_\perp = 2.252$	$A_\perp = 55$
		−0.8 V	$[(TMpyP)Co(py)]^{2+}$	$g_\perp = 2.355$; $g_\parallel$; 1.964	$A_\parallel = 94$; $A_\parallel^N = 16$
py	12[d]	none[c]	$[(TMpyP)Co(py)_2]^{4+}$	$g_{iso} = 2.201$	$A_{iso} = 52$
		−0.8 V	$[(TMpyP)Co(py)_2]^{2+}$	$g_{iso} = 2.213$	$A_{iso} = 53$
Me_2SO	0	none[c]	$[(TMpyP)Co(Me_2SO)]^{4+}$	$g_\perp = 2.317$; $g_\parallel = 2.042$	$A_\parallel = 80$
	2.0	none[c]	$[(TMpyP)Co(Me_2SO)(py)]^{4+}$	$g_\perp = 2.055$	$A_\parallel = 57$

[a] All solvents contained 0.1 M TBAP. [b] Error limits are ±0.002 for g values and ±5% for A values. [c] Stable complex prior to electroreduction. [d] Neat pyridine.

function of TBAP concentration (see insert of Figure 2) consistent with an increased percentage of dissociation. This increase in molar conductance occurs up to a TBAP concentration of about 5×10^{-3}, after which Λ starts to decrease, consistent with an increased ion-pairing interaction between tetravalent $[(TMpyP)Co]^{4+}$ and the ClO_4^- anions from the TBAP supporting electrolyte. The data in Figure 2 thus indicate that ion-paired $(TMpyP)Co(ClO_4)_4$ is the form of the porphyrin present in solutions of DMF containing 0.1 M TBAP. However, for purposes of discussion, all ClO_4^- counterions are omitted in reactions described throughout the text.

Cobalt(II) porphyrins are known to axially coordinate with solvent molecules such as DMF, Me_2SO, and py,[8,10,11] and a similar solvent coordination of $[(TMpyP)Co]^{4+}$ is suggested by literature data for the complex in aqueous media containing amine ligands,[20] as well as by the solvent dependence of the UV–visible and ESR spectral data obtained in this present study. The UV–visible spectrum of $[(TMpyP)Co]^{4+}$ consists of a broad Soret band located between 426 and 440 nm and one visible band located between 537 and 545 nm. Both absorption bands of $[(TMpyP)Co]^{4+}$ shift to higher wavelengths as the Gutmann donor number (DN)[24] of the solvent increases, and this suggests that the cobalt(II) species is present in solution as either five-coordinate $[(TMpyP)Co(S)]^{4+}$ or six-coordinate $[(TMpyP)Co(S)_2]^{4+}$, where S = a solvent molecule.

ESR spectra of $[(TMpyP)Co^{II}]^{4+}$ in neat DMF, in DMF/py mixtures, and in neat py are shown in Figure 3, and a summary of the ESR parameters in different DMF/py mixtures is given in Table I. The ESR spectrum of the complex in neat DMF (Figure 3a) has $g_\parallel = 2.061$ and $g_\perp = 2.335$ and is typical of a five-coordinate Co(II) porphyrin complexed with a Lewis base.[25,26] This spectrum is assigned to $[(TMpyP)Co^{II}(DMF)]^{4+}$.

The addition of 5 equiv of py to $[(TMpyP)Co^{II}(DMF)]^{4+}$ in DMF gives the ESR spectrum shown in Figure 3b, which can be compared to the spectrum obtained for $[(TMpyP)Co]^{4+}$ in water buffered to pH 9.2 with 0.01 M NH_3.[20] The spectrum in Figure 3b is also quite similar to a spectrum reported by Schrauzer and Lee for vitamin B_{12} in aqueous solutions containing an amine ligand.[27] The triplet splitting is resolved in DMF containing 5 equiv of pyridine and indicates the binding of one pyridine ligand to the Co(II) center of $[(TMpyP)Co(DMF)]^{4+}$ as shown by eq 2.

$$[(TMpyP)Co(DMF)]^{4+} + py \rightleftharpoons [(TMpyP)Co(DMF)(py)]^{4+} \quad (2)$$

Both the $g_\parallel$ and $g_\perp$ values of the spectrum change as the pyridine concentration in DMF is increased (see Figure 3c,d) and the ESR spectrum becomes invariant in the region 0.02 M < [py] < 2.0 M. The spectra in this region of py concentration (Figure 3d) are assigned to six-coordinate $[(TMpyP)Co(DMF)(py)]^{4+}$, and this assignment agrees with the results from electrochemical data, which are discussed in a later section of the manuscript. The increased $g_\perp$ value of the initial complex at higher pyridine concentrations is also consistent with a change from five-coordinate $[(TMpyP)Co(DMF)]^{4+}$ to six-coordinate $[(TMpyP)Co^{II}(DMF)(py)]^{4+}$.[28,29]

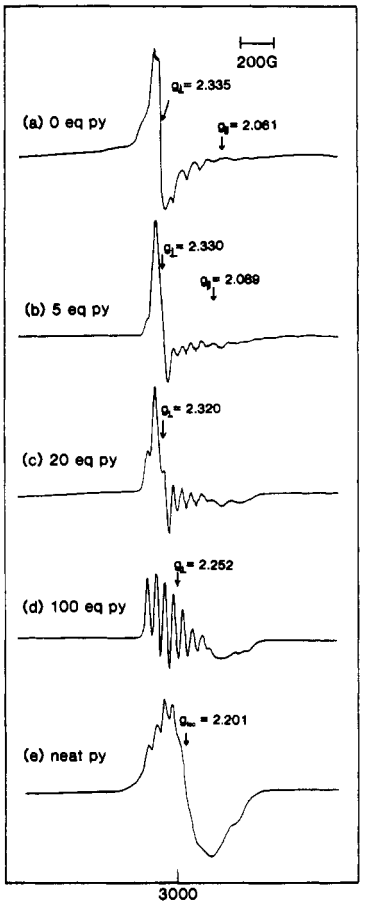

Figure 3. ESR spectra of 4.5×10^{-4} M $[(TMpyP)Co]^{4+}$ in DMF containing 0.1 M TBAP and the following concentrations of py: (1) 0 equiv, (b) 5 equiv, (c) 20 equiv, (d) 100 equiv, and (e) neat py.

The ESR spectrum of $[(TMpyP)Co]^{4+}$ in neat pyridine is shown in Figure 3e. An isotropic signal is centered at $g_{iso} = 2.201$, and the ESR-active species is assigned as $[(TMpyP)Co^{II}(py)_2]^{4+}$. This assignment of a bis(pyridine)cobalt(II) complex in neat pyridine is also consistent with data obtained by analysis of the current voltage curves for the electrochemical reduction and oxidation of the complex in DMF/py mixtures (see following sections).

The ESR spectrum of $[(TMpyP)Co]^{4+}$ in neat Me_2SO has $g_\parallel = 2.042$, $g_\perp = 2.317$, and $A_\parallel = 80$ G, which is consistent with the formation of $[(TMpyP)Co(Me_2SO)]^{4+}$. A titration of this solution with py results in changes similar to those observed during the titration of $[(TMpyP)Co(DMF)]^{4+}$ by pyridine in DMF, and these data are summarized in Table I.

(24) Gutmann, V. *The Donor Acceptor Approach to Molecular Interaction*; Plenum: New York, 1978.
(25) Walker, F. A. *J. Am. Chem. Soc.* **1970**, *92*, 4235.
(26) Subramanian, J. In *Porphyrins and Metalloporphyrins*; Smith, K. M.; Ed.; Elsevier: Amsterdam, 1975; Chapter 13.
(27) Schrauzer, G. N.; Lee, L. P. *J. Am. Chem. Soc.* **1968**, *90*, 6541.
(28) Walker, F. A. *J. Am. Chem. Soc.* **1973**, *95*, 1150.
(29) (a) Scheidt, W. R. *J. Am. Chem. Soc.* **1974**, *96*, 90. (b) Dwyer, P. N.; Madura, P.; Scheidt, W. R. *J. Am. Chem. Soc.* **1974**, *96*, 4815.

Table II. Half-Wave Potentials (V vs SCE) and Peak Potential Differences between E_{pc} and E_{pa} (ΔE_p, mV) for the Electrooxidation/Reduction of $[(TMpyP)Co]^{4+}$ at 0.1 V/s in DMF, Me_2SO, and py Containing 0.1 M TBAP

	redn[a]				oxidn[a]
solvent	reacn I	reacn II	reacn III	reacn IV	reacn V
DMF	−0.49 (80)	−0.71 (80)	−0.89 (40)	−0.98 (42)	~0.25 (...)[b]
Me_2SO	−0.53 (70)	−0.69 (75)	−0.95 (...)[c]	−1.02 (...)[c]	0.26 (100)
py	−0.61 (40)[d]	−0.61 (40)[d]	−0.91 (25)[e]	−0.91 (25)[e]	−0.01 (65)

[a] See text, Figure 3, and Figure 4 for a description of each electrode reaction. [b] Poorly defined peak (see Figures 5a and 8a). [c] ΔE_p could not be determined for overlapping peaks. [d] Reactions I and II are overlapped to give a single reduction at $E_{1/2}$ = −0.61 V. [e] Reactions III and IV are overlapped to give a single reduction at $E_{1/2}$ = −0.91 V.

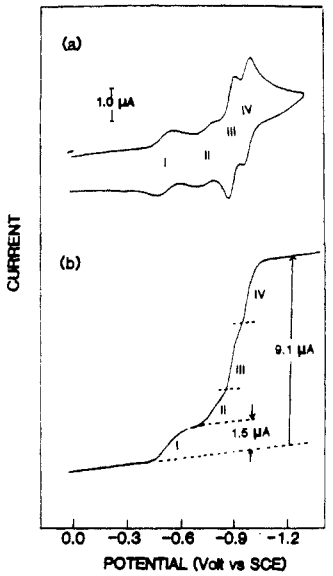

Figure 4. (a) Cyclic voltammogram and (b) normal-pulse voltammogram illustrating the reduction of $[(TMpyP)Co]^{4+}$ in DMF containing 0.1 M TBAP.

Electrochemistry of $[(TMpyP)Co]^{4+}$ in DMF, Me_2SO, and py. Cyclic and normal-pulse voltammograms for the reduction of $[(TMpyP)Co]^{4+}$ in DMF are shown in Figure 4. Four reductions occur between 0.0 and −1.25 V and these are labeled as processes I–IV. The ΔE_p values, $|E_{pa} - E_{pc}|$, for the first process vary between 70 and 80 mV by cyclic voltammetry (Figure 3a) and the peak current, i_p, is proportional to the square root of scan rate. These data suggest a quasireversible diffusion-controlled one-electron transfer in the first reduction.

Processes II and III are partially overlapped but the $|E_{pa} - E_{pc}| \approx 75 \pm 5$ mV for the first reduction by cyclic voltammetry also suggests a quasireversible one-electron transfer. On the other hand, the $\Delta E_p = 40 \pm 2$ mV value for processes III and IV (at a scan rate of 0.1 V/s) suggests a two-elctron transfer in each step. The peak current for these two reductions by cyclic voltammetry increases linearly with the square root of scan rate, indicating diffusion-controlled reactions.

The normal pulse voltammogram of $[(TMpyP)Co]^{4+}$ (Figure 4b) has a maximum peak current of 1.5 μA for process I, which is one-sixth of the total 9.1-μA limiting current. This result is consistent with the cyclic voltammetric data in Figure 4a, which indicates a one-electron transfer in the first step and the overall addition of five additional electrons in processes II–IV.

The electroreduction of $[(TMpyP)Co]^{4+}$ was also monitored in Me_2SO and py. Differential-pulse voltammograms in these three solvents are shown in Figure 5, and a summary of $E_{1/2}$ values by cyclic voltammetry in each solvent is given in Table II. As seen in Figure 5 and Table II, the potential for the reduction process I progressively shifts negatively while that for process II shifts positively upon going from DMF to Me_2SO to py as a solvent. The peak potential difference between the first two reductions of $[(TMpyP)Co]^{4+}$ by differential-pulse voltammetry is 234 mV in DMF (Figure 5a), 172 mV in Me_2SO (Figure 5b), and 0 mV in neat pyridine (Figure 5c) where the first reduction involves an overall two-electron-transfer step.

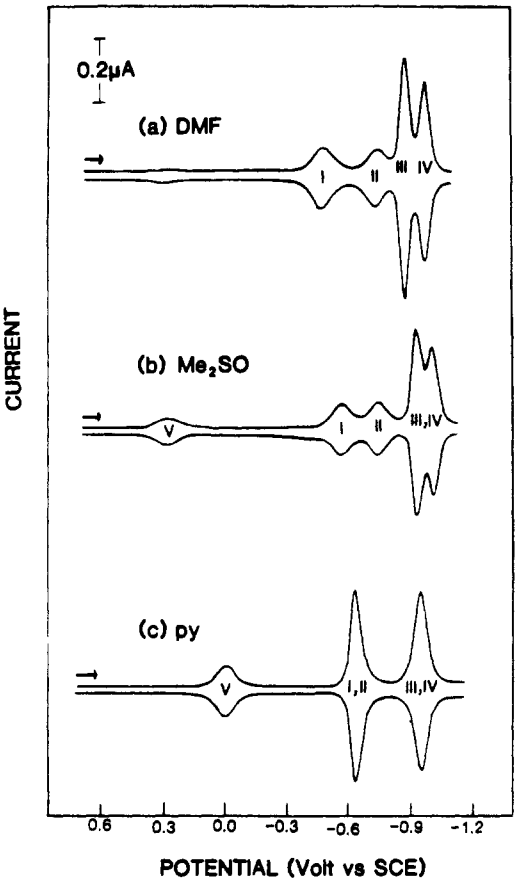

Figure 5. Differential-pulse voltammograms of $[(TMpyP)Co]^{4+}$ in (a) DMF, (b) Me_2SO, and (c) py containing 0.1 M TBAP.

The number of electrons transferred in each electroreduction of $[(TMpyP)Co]^{4+}$ was verified by both thin-layer and bulk controlled-potential coulometry. Both bulk and thin-layer controlled-potential electrolysis at −1.25 V gave an overall n = 6.0 ± 0.5 in all three solvents. This reduction was reversible by thin-layer coulometry (n = 5.8 ± 0.2) but not by bulk electrolysis where an $n \simeq 4.4 \pm 0.4$ obtained upon reoxidation. Fresh solutions of $[(TMpyP)Co]^{4+}$ in DMF or Me_2SO gave an n = 1.0 ± 0.1 upon reduction at −0.60 V and an n = 2.0 ± 0.2 upon reduction at −0.85 V, and these values compare with an n = 2.0 ± 0.2 for reduction of the same complex by two electrons at −0.75 V in neat py.

The first two reductions of $[(TMpyP)Co]^{4+}$ are reversible on the thin-layer timescale as is the first reduction process I on the bulk controlled-potential electrolysis time scale. However, as already mentioned, the return coulometric value for reoxidation of reduced $[(TMpyP)Co]^{4+}$ was low when the bulk reduction was carried out at potentials negative of −0.70 V. Under these conditions, the electrogenerated species adsorbs on the electrode surface. A similar adsorption of the reduction product was reported for electroreduced $[(TMpyP)M]^{4+}$ in DMF where M = Cu(II), Zn(II), and VO.[13]

$[(TMpyP)Co]^{4+}$ undergoes only one oxidation between 0.0 and 1.0 V in DMF, Me_2SO, or py. The $E_{1/2}$ for this reaction (labeled process V in Figure 5) ranges between +0.30 and −0.20 V in the

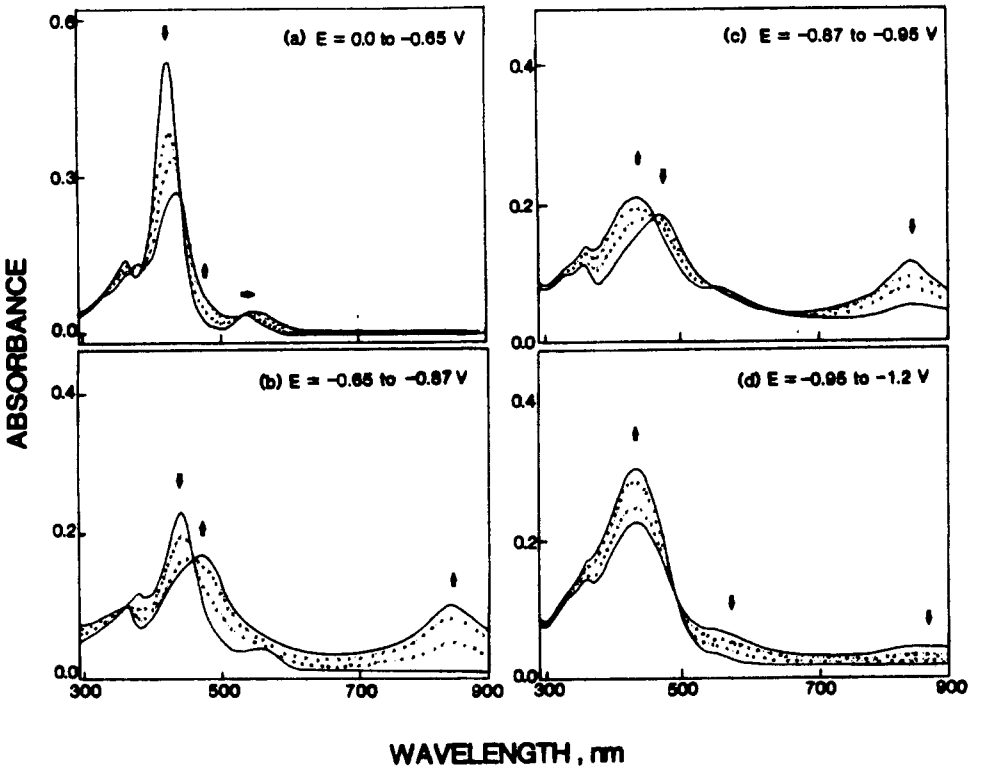

Figure 6. Thin-layer spectral changes obtained upon the stepwise reduction of $[(TMpyP)Co]^{4+}$ in DMF containing 0.1 M TBAP by (a) one electron, (b) two electrons, (c) four electrons, and (d) six electrons.

three investigated solvents and compares with $E_{1/2}$ values for the Co(II)/Co(III) reaction of other (P)Co complexes under the same solution conditions.[1,5,6-9] The oxidation of $[(TMpyP)Co]^{4+}$ is poorly defined by differential-pulse polarography in DMF (see Figure 5a), but the currents for this reaction increase substantially upon going to neat Me_2SO (Figure 5b) or neat py (Figure 5c). A similar decreased current and irreversibility of the Co(II)/Co(III) reaction has been reported for the oxidation of (TPP)Co and $((CN)_4TPP)Co$ in DMF[8,10,11] and this has been attributed to a slow rate-determining step in the electrochemical conversion of the five-coordinate Co(II) porphyrin to the six-coordinate Co(III)–DMF adduct.

Identification of Electrooxidation/Reduction Products. The UV–visible spectral changes obtained upon the stepwise six-electron reduction of $[(TMpyP)Co]^{4+}$ in DMF are shown in Figure 6, and a summary of spectral data before and after each electroreduction step is given in Table III. During the first one-electron reduction (Figure 6a), the Soret band decreases in intensity and new bands grow in at 434 and 545 nm. There are no absorption bands between 650 and 750 nm, suggesting the formation of a Co(I) species rather than a cobalt(II) porphyrin π radical.[30] The one-electron-reduced species is ESR inactive and the overall reaction appears to proceed as shown in eq 3. The

$$[(TMpyP)Co^{II}(DMF)]^{4+} + e^- \rightleftarrows [(TMpyP)Co^{I}]^{3+} + DMF \quad (3)$$

binding of one DMF ligand to $[(TMpyP)Co]^{4+}$ and the loss of this axial ligand upon formation of $[(TMpyP)Co^{I}]^{3+}$ are consistent with results for other $(P)Co^{II}$ and $[(P)Co^{I}]^-$ species in the literature.[1,6,8,10,11] Additional evidence for the formation of Co(I) in reaction 2 is also given by the reaction of the electroreduced product with CH_3I to generate $[(TMpyP)Co(CH_3)]^{4+}$. These reactions and a characterization of the σ-bonded product will be discussed in a separate manuscript.

Thin-layer spectral changes obtained during the second one-electron reduction of $[(TMpyP)Co]^{4+}$ in DMF are shown in Figure 6b. The final spectrum has broad peaks centered at 469 and 835 nm and is similar to the spectra obtained after a two-electron reduction of $[(TMpyP)Cu]^{4+}$, $[(TMpyP)Zn]^{4+}$, or $[(TMpyP)VO]^{4+}$ in DMF.[13] The spectral products after the third and fourth two-electron reductions of $[(TMpyP)Co]^{4+}$ (Figure 6c,d) are also similar to spectra obtained after the second and third two-electron reductions of $[(TMpyP)M]^{4+}$ (M = Cu(II), Zn(II), or VO) in DMF.[13] These latter reactions have been characterized as occurring at the *N*-methylpyridiniumyl substituents of TMpyP, and the similarity of these spectra to those in Figures 6c and 6d suggest that processes III and IV involve an overall four-electron reduction at the *N*-methylpyridiniumyl substituents of $[(TMpyP)Co]^{2+}$. An ESR spectrum of the six-electron-reduced product is given in later sections of the paper and is also consistent with the formation of a Co(II) species as the final electroreduction product.

The oxidation of $[(TMpyP)Co]^{4+}$ by one electron leads to the UV–visible changes shown in Figure 7 and gives results similar to those observed upon the electrogeneration of other cobalt(III)

Table III. UV–Visible Spectra for the Oxidation/Reduction Products of $[(TMpyP)Co]^{4+}$ in DMF, Me_2SO and py, Containing 0.1 M TBAP

solvent	process	electrode reacn (n)[a]	λ, nm ($10^{-3}\epsilon$)	
DMF	none[b]	none[b]	426 (101)	537 (9.0)
	I	1st redn (1)	434 (56.9)	545 (9.6)
	II	2nd redn (1)	469 (35.0)	835 (22.9)
	III	3rd redn (2)	438 (42.9)	840 (7.9)
	IV	4th redn (2)	439 (57.3)	
	V	1st oxidn (1)	441 (105)	558 (11.7)
Me_2SO	none[b]	none[b]	433 (104)	545 (10.0)
	I	1st redn (1)	426 (60.7)	536 (6.6)
	II	2nd redn (1)	468 (39.9)	844 (31.4)
	III	3rd redn (2)	429 (42.5)	861 (11.1)
	IV	4th redn (2)	427 (55.0)	
	V	1st oxidn (1)	441 (101)	558 (10.1)
py	none[b]	none[b]	440 (102)	542 (13.1)
	I,II	1st redn (2)	431 (48.3)	851 (19.6)
	III,IV	2nd redn (4)	434 (61.5)	
	V	1st oxidn (1)	443 (121)	556 (14.7)

[a] n gives the coulometric number of electrons involved in the oxidation/reduction step. [b] Initial complex before oxidation or reduction.

(30) Gouterman, M. In *The Porphyrins*; Dolphin, D., Ed.; Academic Press: New York, 1979; Vol. III, Chapter 7.

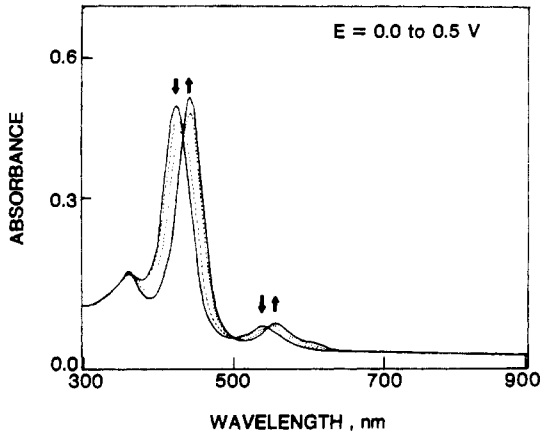

Figure 7. Thin-layer spectral changes obtained upon the oxidation of $[(TMpyP)Co]^{4+}$ in DMF containing 0.1 M TBAP. The potential was scanned from 0.0 to 0.5 V.

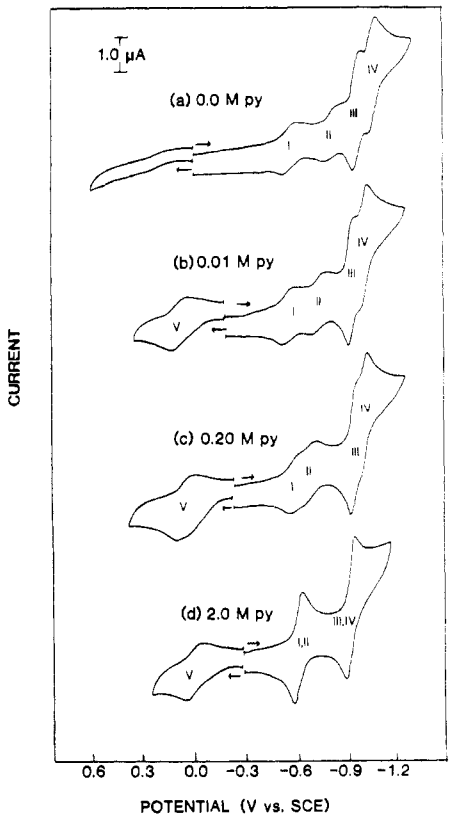

Figure 8. Cyclic voltammograms of $[(TMpyP)Co]^{4+}$ in DMF containing 0.1 M TBAP and the following concentrations of py: (a) 0.0 M, (b) 0.01 M, (c) 0.20 M, and (d) 2.0 M.

porphyrins in DMF.[31] Both the Soret and visible bands of the Co(II) porphyrin shift to higher wavelengths upon generation of Co(III) and the spectral properties of $[(TMpyP)Co^{III}(S)_2]^{5+}$ in all three solvents are summarized in Table III. As expected, the final product formed after the one-electron oxidation of $[(TMpyP)Co]^{4+}$ at 0.50 V is ESR inactive.

Electrochemistry of $[(TMpyP)Co]^{4+}$ in DMF/py Mixtures. Cyclic voltammograms of $[(TMpyP)Co]^{4+}$ in DMF solutions containing various concentrations of py are shown in Figure 8, and plots of $E_{1/2}$ vs log [py] for each reduction/oxidation are shown in Figure 9. This latter figure is divided into three concentration regions labeled as regions A–C. Region A is for $[py] < 6.0 \times 10^{-3}$ M, Region B is for $6.0 \times 10^{-3} < [py] < 5 \times 10^{-1}$ M, and Region C is for [py] > 0.5 M. The ESR data presented in earlier sections of the paper suggest that $[(TMpyP)Co(DMF)]^{4+}$

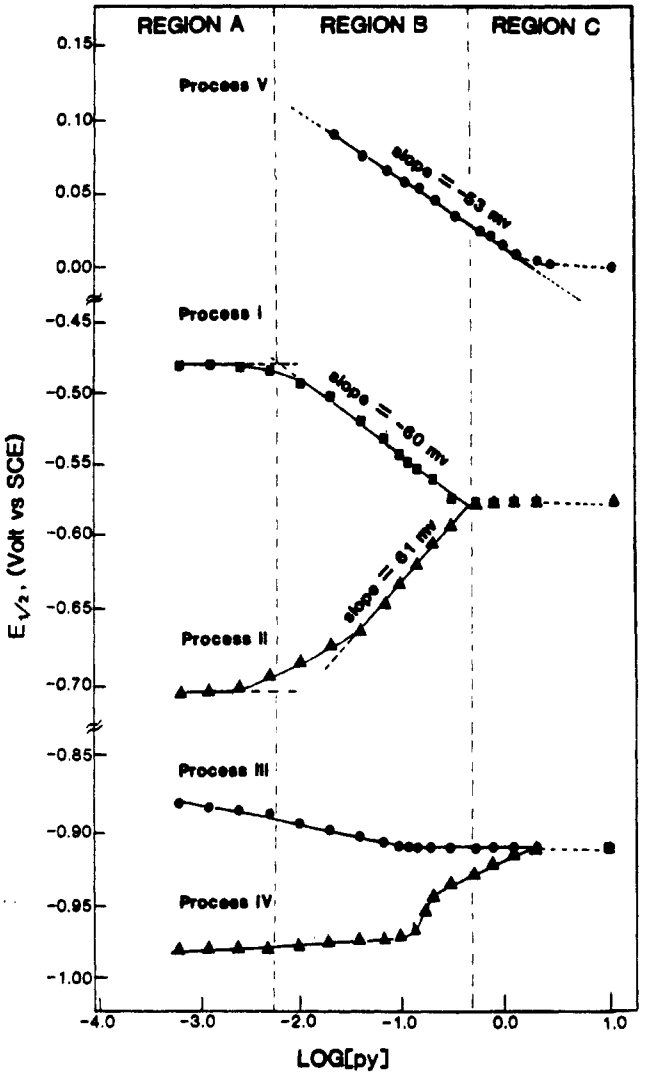

Figure 9. Plot of half-wave potential vs log [py] for the electrode reactions of $[(TMpyP)Co]^{4+}$ in DMF containing 0.1 M TBAP.

is present both in pure DMF and in DMF/py concentrations over region A (see Figure 3b). The ESR data also suggest that $[(TMpyP)Co(DMF)(py)]^{4+}$ is present in regions B and C (see Figure 3d) and that $[(TMpyP)Co(py)_2]^{4+}$ is present in neat pyridine or when [py] > 2.0 M (see Figure 3e).

Half-wave potentials for the electroreduction processes I–IV in region A are insensitive to changes in py concentration. The slope of $E_{1/2}$ vs log [py] is close to zero for all four processes, indicating the absence of a py ligand exchange during the electron-transfer step as well as a lack of py binding to the neutral or reduced species. The oxidation process V is ill-defined in region A (see voltammograms in Figures 5a and 8a), and an $E_{1/2}$ value is thus not easily obtained either in neat DMF or in DMF containing less than 10^{-2} M py. However, the electrooxidation of $[(TMpyP)Co]^{4+}$ becomes well-defined in solutions of DMF containing $[py] \geq 10^{-2}$ M, and this is shown by the cyclic voltammograms in Figure 8b–d.

Experimental slopes of −53 and −60 mV/log [py] are obtained for process V and process I in Region B. Both values are consistent with the exchange of one py ligand during the electron-transfer step and agree with electrochemical data in the literature for other Co(II) and Co(III) porphyrins in DMF/py mixtures[11] where the electrode reactions are given by reactions 4 and 5.

$$[(TMpyP)Co^{II}(DMF)(py)]^{4+} + py \rightleftarrows [(TMpyP)Co^{III}(py)_2]^{5+} + e^- + DMF \quad (4)$$

$$[(TMpyP)Co^{II}(DMF)(py)]^{4+} + e^- \rightleftarrows [(TMpyP)Co^{I}]^{3+} + py + DMF \quad (5)$$

(31) Kadish, K. M.; Lin, X. Q.; Han, B. C. *Inorg. Chem.* **1987**, *26*, 4161.

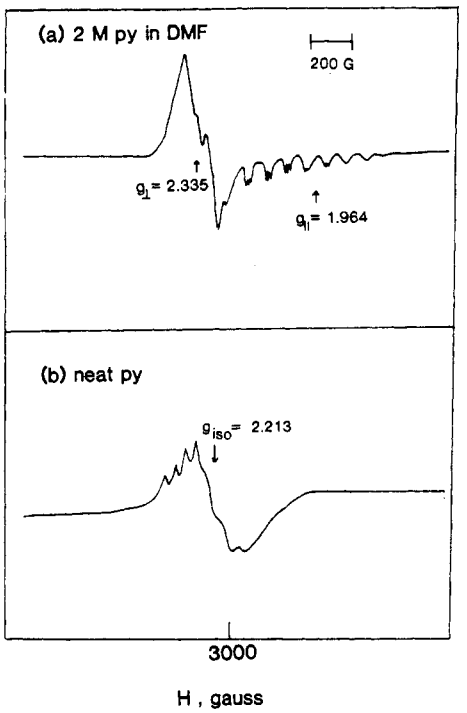

Figure 10. ESR spectra of $[(TMpyP)Co]^{4+}$ after electrolysis by two electrons at −0.80 V (a) in DMF containing 2.0 M py and 0.1 M TBAP and (b) in neat py containing 0.1 M TBAP.

In contrast to the −60-mV slope for process I in region B, the reduction process II has a slope of +61 mV/log [py] which suggests the binding of one py ligand upon the reversible one-electron reduction of $[(TMpyP)Co^{I}]^{3+}$. The most obvious reaction consistent with this slope is given by eq 6, but the actual overall

$$[(TMpyP)Co^{I}]^{3+} + e^- + py \rightleftarrows [(TMpyP)Co^{I}(py)]^{2+} \quad (6)$$

sequence of steps more likely involves the overall mechanism shown by eq 7. In this equation, the overall change on the complex is

$$[(TMpyP)Co^{I}]^{3+} + e^- + py \rightleftarrows [(TMpyP)Co^{II}(py)]^{2+} \quad (7)$$

reduced by one electron, but the site of reduction changes from the Co center in $[(TMpyP)Co^{I}]^{2+}$ to the porphyrin π-ring system in $[(TMpyP)Co^{II}(py)]^{2+}$. This process may or may not involve formation of transient $[(TMpyP)Co^{I}]^{2+}$ or $[(TMpyP)Co^{II}]^{2+}$ before complexation of one py ligand.

Processes I and II in Figure 9 merge into a single process at [py] > 0.5 M (region C), and under these experimental conditions, the overall two-electron reduction at $E_{1/2}$ = −0.61 V is given by eq 8, which is a simple combination of eqs 5 and 7. The lack of

$$[(TMpyP)Co^{II}(DMF)(py)]^{4+} + 2e^- \rightleftarrows [(TMpyP)Co^{II}(py)]^{2+} + DMF \quad (8)$$

an $E_{1/2}$ shift with change in py concentration in this region suggests that neither a binding nor a loss of a pyridine ligand occurs during the electroreduction.

Evidence for six-coordinate $[(TMpyP)Co(DMF)(py)]^{4+}$ as a reactant and five-coordinate $[(TMpyP)Co^{II}(py)]^{2+}$ as a final product in eq 8 derives from ESR measurements carried out after controlled-potential reduction of the initial $[(TMpyP)Co]^{4+}$ species at −0.85 V in DMF containing 2.0 M py. The resulting ESR spectrum is shown in Figure 10a and differs substantially from the spectrum of the Co(II) complex before electroreduction (see Figure 3d). The spectrum of the reduced porphyrin (Figure 10a) has an axial symmetry of **g** tensors with $g_\parallel$ = 1.964, $g_\perp$ = 2.355, $A_\perp$ = 94 G, and a superhyperfine nitrogen splitting, $A_\parallel$ = 16 G. These data are summarized in Table I and are consistent with the formation of five-coordinate $[(TMpyP)Co^{II}(py)]^{2+}$ after a two-electron reduction of $[(TMpyP)Co^{II}(DMF)(py)]^{4+}$ under the given experimental conditions.

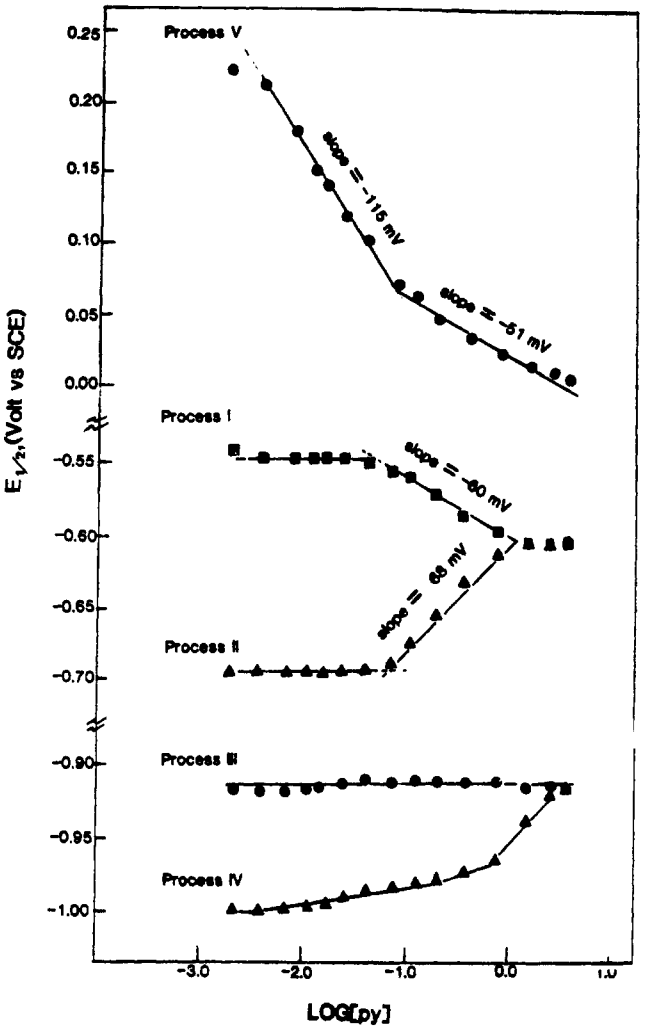

Figure 11. Plot of half-wave potential vs log [py] for the electrode reactions of $[(TMpyP)Co]^{4+}$ in Me_2SO containing 0.1 M TBAP.

The ESR data in neat py (Figure 10b) indicates that the bis(pyridine) adduct, $[(TMpyP)Co(py)_2]^{2+}$, is formed after a two-electron reduction of $[(TMpyP)Co(py)_2]^{4+}$. Under these solution conditions, there is an isotropic spectrum centered at g_{iso} = 2.213, and this spectrum is similar to the one obtained for $[(TMpyP)Co(py)_2]^{4+}$ before electrolysis (see Figure 3e). Both the ESR and electrochemical data are thus self-consistent with the occurrence of the following electrode reaction in neat pyridine.

$$[(TMpyP)Co^{II}(py)_2]^{4+} + 2e^- \rightleftarrows [(TMpyP)Co^{II}(py)_2]^{2+} \quad (9)$$

The $E_{1/2}$ values for reduction processes III and IV shift only slightly in DMF containing less than 10^{-1} M py (region B) but begin to merge into a single overlapping peak as the py concentration approaches 1.0 M (region C). This overlap is complete at ≃2.0 M py and under these conditions the cyclic voltammogram illustrated in Figure 8d is obtained. This voltammogram is well-defined and involves an overall four-electron reduction of $[(TMpyP)Co^{II}(py)]^{2+}$ in the first step as confirmed by controlled-potential coulometry at −1.25 V.

Electrochemistry of $[(TMpyP)Co]^{4+}$ in Me_2SO/py Mixtures. The electrochemistry of $[(TMpyP)Co]^{4+}$ in Me_2SO/py mixtures is similar to but not identical with that observed in DMF/py mixtures. The initial compound undergoes four diffusion-controlled reductions and one diffusion-controlled oxidation in Me_2SO as illustrated by the differential-pulse voltammogram in Figure 5b. The first two reductions each involve a one-electron addition while the first oxidation of the complex involves a one-electron abstraction to give solvated $[(TMpyP)Co(Me_2SO)_2]^{5+}$ as a final product. Both the third and the fourth reductions involve a two-electron-transfer step, and this was verified by controlled-

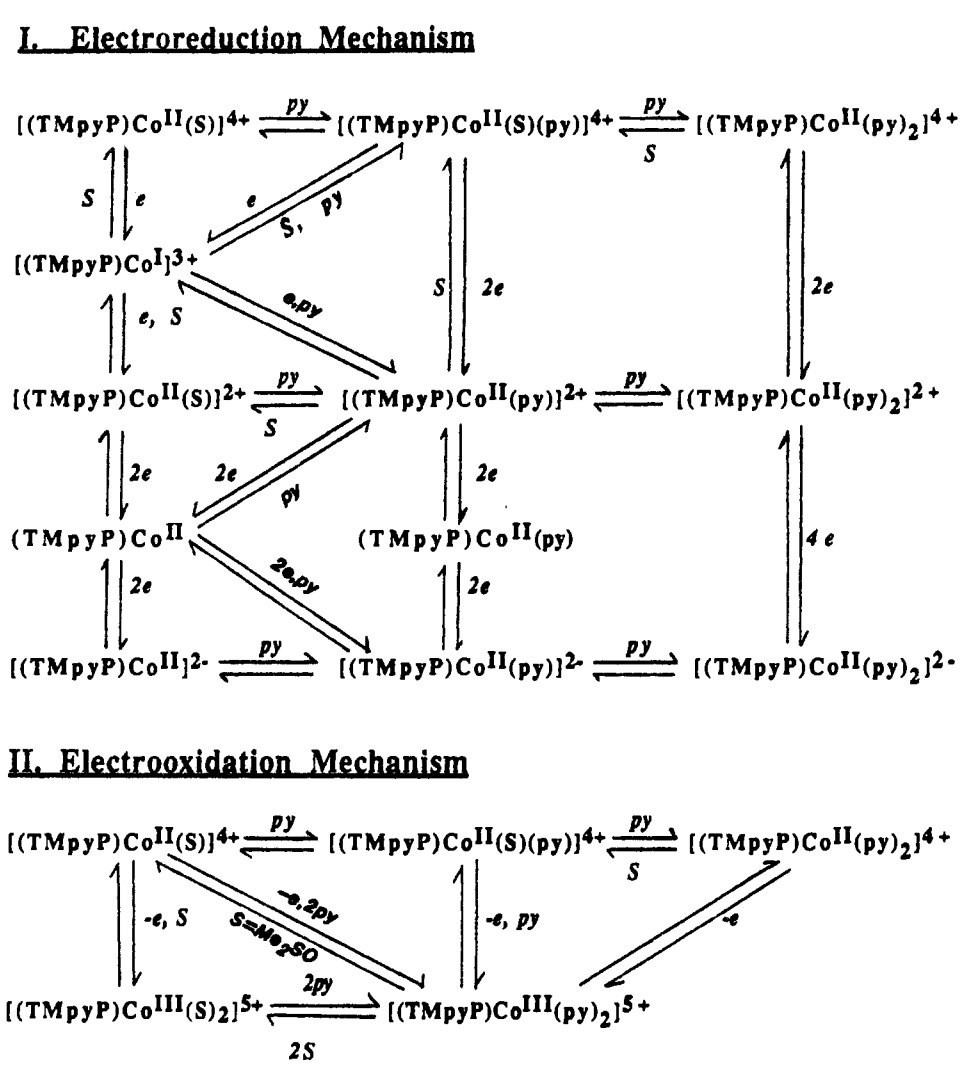

Figure 12. Overall electron-transfer mechanism for $[(TMpyP)Co]^{4+}$ in DMF, Me_2SO, or pyridine.

potential coulometry, which is discussed in earlier sections of the paper.

Plots of $E_{1/2}$ vs log [py] for the reduction of $[(TMpyP)Co]^{4+}$ in Me_2SO are shown in Figure 11 and are qualitatively similar to the data shown in Figure 9. In Me_2SO solutions containing 3×10^{-3} to 5×10^{-2} M py, the first oxidation (process V) shifts by −115 mV per 10-fold charge in py concentration while processes I and II have a constant $E_{1/2}$ value. This behavior is similar to that of (TPP)Co in Me_2SO/py mixtures[11] and is consistent with an electrode reaction involving the formation of $[(TMpyP)Co(py)_2]^{5+}$ from $[(TMpyP)Co(Me_2SO)]^{4+}$ as shown by eq 10.

$$[(TMpyP)Co^{II}(Me_2SO)]^{4+} + 2py \rightleftarrows [(TMpyP)Co^{III}(py)_2]^{5+} + Me_2SO + e^- \quad (10)$$

$[(TMpyP)Co(Me_2SO)(py)]^{4+}$ is formed in solution when the py concentration in Me_2SO is increased above 0.05 M, and under these conditions, the slopes of $E_{1/2}$ vs log [py], for processes V, I, and II are −51, −60, and +68 mV, respectively. All three values are similar to slopes obtained in region B of Figure 9. Peaks I and II are merged into a single two-electron-reduction step in Me_2SO containing [py] > 1 M, and peaks III and IV are merged into an overall four-electron-reduction step in solutions where [py] > 1.5 M. Under these solution conditions, the resulting cyclic voltammogram is virtually identical with the one shown in Figure 8d, and with the exception of process V, the overall reduction mechanism is also identical with the one obtained in DMF/py mixtures. This reduction mechanism is summarized in Figure 12, where S = Me_2SO or DMF.

Formation Constants for Pyridine Binding to the Neutral, Oxidized, and Reduced Forms of $[(TMpyP)Co]^{4+}$. Formation constants for pyridine binding to the different Co(II) and Co(III) complexes in DMF or Me_2SO were calculated from electrochemical data of the type shown in Figures 9 and 11 by using eq 11.[32] In the above equation, $E_{1/2}(c)$ and $E_{1/2}(s)$ are reversible

$$E_{1/2}(c) = E_{1/2}(s) - \frac{0.059}{n} \log \frac{K_{ox}}{K_{red}} - \frac{0.059}{n} \log [L]^{p-q} \quad (11)$$

half-wave potentials of the complexed and uncomplexed oxidized and reduced species, K_{ox} and K_{red} are formation constants for the oxidized and reduced species, [L] is the free concentration of py in solution, p and q are the number of pyridine ligands bound to the oxidized and reduced species, respectively, and n is the number

Table IV. Formation Constants for the Binding of Pyridine to Neutral, Oxidized, and Reduced Cobalt Porphyrins in DMF or Me_2SO

eq	solvent (S) DMF	Me_2SO
$[(TMpyP)Co^{III}(S)_2]^{5+} + 2py \rightleftarrows [(TMpyP)Co^{III}(py)_2]^{5+} + 2S$	6.80	4.8
$[(TPP)Co^{III}(S)_2]^+ + 2py \rightleftarrows [(TPP)Co^{III}(py)_2]^+ + 2S$	9.1[a]	5.9[a]
$[(TMpyP)Co^{II}(S)]^{4+} + py \rightleftarrows [(TMpyP)Co^{II}(S)(py)]^{4+}$	2.14	1.42
$(TPP)Co^{II}(S) + py \rightleftarrows (TPP)Co^{II}(py) + S$	2.07[a]	2.14[a]
$[(TMPyP)Co^{II}(S)]^{2+} + py \rightleftarrows [(TMpyP)Co^{II}(py)]^{2+} + S$	2.18	1.76
$[(TPP)Co^{I}]^{2-} + py \rightleftarrows$ NR[b]		

[a] Reference 11. [b] NR = no reaction.

(32) Kolthoff, I. M.; Lingane, J. J. In *Polarography*, 2nd ed.; Interscience: New York, 1952; Vol. I, p 66.

of electrons involved in a given diffusion-controlled electron-transfer step.

The calculated values of formation constants from eq 11 are summarized in Table IV, which also lists literature values for py binding to neutral and oxidized (TPP)Co under similar experimental conditions. One might expect to observe higher py binding constants to the charged TMpyP complex due to the macrocycle's electron-withdrawing properties.[8,13] However, this is not the case in DMF or Me_2SO and suggests that the solvated ligands (DMF or Me_2SO) that are displaced by py are more tightly bound to the TMpyP cobalt complexes then to the TPP cobalt derivatives. A binding of py to the doubly reduced $[(TPP)Co]^{2-}$ is not observed, but formation constants of 58 M^{-1} and 151 M^{-1} were calculated for the binding of py to doubly reduced $[(TMpyP)Co]^{2+}$ in Me_2SO and DMF, respectively.

Summary. The mechanism for oxidation or reduction of $[(TMpyP)Co]^{4+}$ in DMF, Me_2SO, or py involves three or five electron-transfer steps, all of which occur in a potential range of +0.4 to -1.20 V. Unlike $[(TMpyP)M]^{4+}$ complexes where M = Cu(II), Zn(II), and VO, $[(TMpyP)Co]^{4+}$ undergoes an oxidative process and this step involves the removal of one electron from Co(II) to generate the solvated $[(TMpyP)Co^{III}(S)_2]^{5+}$ species. No porphyrin ring oxidation is observed up to potentials of +1.0 V, and this behavior is consistent with that of $[(TMpyP)Cu]^{4+}$, $[(TMpyP)VO]^{4+}$, or $[(TMpyP)Zn]^{4+}$ under similar experimental conditions.

The reduction of $[(TMpyP)Co]^{4+}$ in DMF, Me_2SO, or py involves a total of six electrons, all of which are added to the complex at potentials between -0.4 and -1.2 V vs SCE. Electrochemical and spectral data indicate that the first one-electron reduction involves electron addition to the Co(II) center while the second one-electron reduction involves an electron addition to the porphyrin π-ring system. An intramolecular electron transfer occurs after electroreduction of $[(TMpyP)Co^{I}]^{3+}$ in py solutions, and this reaction leads to $[(TMpyP)Co^{II}(py)]^{2+}$, which was characterized by ESR spectroscopy. Two consecutive reversible two-electron reductions are observed in the potential range of -0.90 to -1.10 V, and these reactions are due to an electroreduction of the four *N*-methylpyridiniumyl groups.

The very facile porphyrin ring reduction of $[(TMpyP)Co]^{4+}$ (process II) is similar to the facile ring reductions of other $[(TMpyP)M]^{4+}$ complexes which are shifted by up to 1200 mV with respect to the (TPP)M derivatives under the same experimental conditions. However, much smaller shifts occur for the metal-centered reductions. These shifts range between 200 and 250 mV for the Co^{II}/Co^{III} reaction and between 320 and 350 mV for the Co^{II}/Co^{I} reaction in the three investigated solvents. The difference in $E_{1/2}$ shifts between the first and the second reduction suggests that the effect of the four *N*-methylpyridiniumyl substituents is to lower the energy levels of the porphyrin e_g orbitals as well as the metal d_{z^2} orbitals to a lesser extent.

Studies of other ionic $[(TMpyP)M]^{5+}$ and metal-carbon-bonded $[(TMpyP)M(R)]^{4+}$ derivatives are now underway to see if similar substituent effects will be observed for complexes with different metals and with different types of metal-ligand binding.

Acknowledgment. The support of the National Institutes of Health (Grant GM 25172) and the National Science Foundation (Grant CHE-8515411) is gratefully acknowledged. We also acknowledge the help of J.-M. Barbe and G. B. Maiya in an initial synthesis of $[(TMpyP)Co]^{4+}$.

Registry No. DMF, 68-12-2; py, 110-86-1; TBAP, 2537-36-2; $[(TMpyP)Co(DMF)]^{4+}$, 127571-98-6; $[(TMpyP)Co(DMF)(py)]^{4+}$, 127571-99-7; $[(TMpyP)Co(py)_2]^{4+}$, 127572-00-3; $[(TMpyP)Co(Me_2SO)]^{4+}$, 127572-01-4; $[(TMpyP)Co(Me_2SO)(py)]^{4+}$, 127572-02-5; $[(TMpyP)Co(py)]^{2+}$, 127572-03-6; $[(TMpyP)Co(py)_2]^{2+}$, 127572-04-7; $[(TMpyP)Co(DMF)]^{2-}$, 127572-05-8; $[(TMpyP)Co(py)_2]^{5+}$, 53993-54-7; $[(TMpyP)Co]^{4+}$, 79346-65-9; $[(TMpyP)Co]^{3+}$, 98938-66-0; $[(TMpyP)Co]^{2+}$, 98938-66-0; $[(TMpyP)Co]$, 127594-03-0; $[(TMpyP)Co]^{2-}$, 127594-34-7; $[(TMpyP)Co]^{5+}$, 51329-41-0; Me_2SO, 67-68-5.

Contribution from the Department of Chemistry, Purdue University, West Lafayette, Indiana 47907

Non-Metal Redox Kinetics: Hypochlorite and Hypochlorous Acid Reactions with Cyanide

Cynthia M. Gerritsen and Dale W. Margerum*

Received December 18, 1989

The rate expression for OCl^- oxidation of CN^- is $-d[OCl^-]/dt = (k_1 + k_2/[OH^-])[CN^-][OCl^-]$, where k_1 is 310 M^{-1} s^{-1} and k_2 is 583 s^{-1} (25.0 °C, μ = 1.00 M). The observed inverse $[OH^-]$ dependence is due to the great reactivity of HOCl, which is 3.9 × 10^6 times more reactive than OCl^- with CN^-. The proposed mechanism with HOCl is

$$OCl^- + H_2O \underset{k_{-3}}{\overset{k_3}{\rightleftharpoons}} HOCl + OH^-$$

$$HOCl + CN^- \xrightarrow{k_4} CNCl + OH^-$$

$$CNCl + 2OH^- \rightarrow OCN^- + Cl^- + H_2O$$

where k_4 is 1.22 × 10^9 M^{-1} s^{-1}, on the basis of pK_a = 7.47 for HOCl at μ = 1.00 M, 25.0 °C. At high CN^- concentration the HOCl reaction becomes so fast that proton-transfer reactions from H_2O to OCl^- and from HCN to OCl^-

$$OCl^- + HCN \underset{k_{-5}}{\overset{k_5}{\rightleftharpoons}} HOCl + CN^-$$

contribute to the rate, where the values for k_3 and k_{-3} are 9 × 10^3 s^{-1} and 1.9 × 10^{10} M^{-1} s^{-1} and the values for k_5 and k_{-5} are 2.2 × 10^7 M^{-1} s^{-1} and 6.6 × 10^8 M^{-1} s^{-1}. Rate constants for Cl^+ transfer from HOCl to nucleophiles decrease in value by 10 orders of magnitude with $CN^- \geq SO_3^{2-} > I^- \gg Br^- \gg Cl^-$, in accord with the decrease of anion nucleophilicity.

Introduction

The addition of chlorine or hypochlorite to waste water has long been an established process for the destruction of cyanide.[1-7] Price et al.[8] reported instantaneous formation of CNCl from HOCl and CN^- at pH 8. Eden et al.[9] studied the reaction at pH 11 and found

(1) White, H. A. *J. Chem. Soc. S. Afr.* **1910**, *11*, 15-17.
(2) Watermayer, G. A.; Hoffenberg, S. N. *Witwatersrand Mining Practice*; Transvaal Chamber of Mines: 1932; pp 459-462.
(3) Bezzubets, M. K.; Vozhdaeva, V. N. *J. Ind. Chim. Moscou* **1941**, *18*, 17.
(4) Meinck, F. *Metallwaren-Ind. Galvanotech.* **1942**, *40*, 225-229.
(5) Friel, F. S.; Wiest, G. J. *Water Works Sewerage* **1945**, *92*, 97-98.
(6) Dobson, J. G. *Sewage Works J.* **1947**, *19*, 1007-1020.

0020-1669/90/1329-2757$02.50/0